CHALLENGES ABOUT DETECTING AND ANALYSING THE ROTOR BLADE TIP VORTICES IN NUMERICAL SIMULATIONS AT LATE WAKE AGES

Filippo Gajo, Manuel Keßler

Institute of Aerodynamics and Gasdynamics
University of Stuttgart, Wankelstraße 3, 70563 Stuttgart, Germany
(filippo.gajo, manuel.kessler)@iag.uni-stuttgart.de

Abstract

Main tip vortex (MTV) are a fundamental feature of a rotor wake for efficiency, noise production and vibrations. During the decay of the wake, the initial helicoidal structure is eventually developing into a complex vortical flow field. To study numerically the late wake age regime, which are of great practical interest to understand the wake decay, difficulties are related to the correct detection of the MTV. Thus, an automated and easily applicable procedure to track the MTV is proposed. This method, through a series of precautions and considerations, allows to follow the MTV even far from the rotor plane. The results, in terms of position, wandering, dimensions and shape of the MTV can be useful regarding a turbulent regime otherwise difficult to analyse.

1. NOTATION

Symbols

$\Gamma\ [m^2/s]$	circulation
$\omega\ [1/s]$	vorticity
$\Omega\ [1/s]$	rotor angular velocity
$V_{tip}\ [m/s]$	blade tip velocity
$V_h\ [m/s]$	induced velocity
$V_\theta\ [m/s]$	tangential velocity in the vortex core
$V_{axial}\ [m/s]$	axial velocity in the vortex core
$f\ [Hz]$	rotation frequency of the rotor
$T\ [N]$	total thrust of the rotor
C_T	thrust coefficient of the rotor
C_T/σ	blade loading
$L\ [N]$	blade span-wise lift
σ	solidity of the rotor
Σ	standard deviation
$\overline{\Sigma}$	standard deviation threshold
Ξ	Covariance matrix
ξ	integration path for circulation
$R\ [m]$	Radius of the rotor
$A_{rot}\ [m^2]$	rotor area
$R_\xi\ [m]$	Radius of integration for circulation
$C\ [m]$	Chord of the blade
N_b	number of blades
N_v	number of secondary structures
λ_2	λ_2-criterion
$\Psi\ [deg]$	Vortex age
$\Psi_{decay}\ [deg]$	Vortex age decay
$\Phi\ [deg]$	azimuth angle of the blade
$\theta_t\ [deg]$	blade twist
$(r_0, z_0)\ [m]$	initial position of the CoG of the MTV
$(r, z)\ [m]$	position of the CoG of the MTV
$(r_c, z_c)\ [m])$	position of the vortex center
$A_{MTV}\ [m^2]$	MTV area estimation
$\Lambda\ [m]$	eigenvalues of the MTV

Acronyms:

IAG	Institute of Aerodynamics and Gasdynamics
DLR	German Aerospace Center
WENO	Weighted Essentially Non-Oscillatory
DDES	Delayed Detached Eddy Simulation
RANS	Reynolds Averaged Navier-Stokes equations
SST	Shear Stress Transport
MTV	Main Tip Vortex
CoG	Center of Gravity (of λ_2)
BPF $[Hz]$	Blade Passage Frequency

2. INTRODUCTION

The main tip vortices (MTV) created by the rotation of the blades are the dominant vortical structure of the flow in a rotor wake. The interest is related firstly to the possible interactions of the wake and other structures of the rotorcraft and, secondly, to safety considerations in particular flight conditions, i.e. near the ground. Specifically, the main tip vortex (MTV) decay is fundamental because it affects the efficiency and the noise production of rotors, especially in hover conditions.

The flow under consideration is characterized by a complex, unsteady, three-dimensional structure where strong interactions of vortical structures are present. The complexity of these interactions and the following breakdown of the wake is still a challenge for high resolution numerical simulation and therefore is the subject of many investigations (i.e. Chaderjian and Buning [1] or Hariharan et al. [2]). In particular, the MTV, which is well defined at early wake stages, increasingly interacts with the blade shear layers and eventually decomposes in a highly turbulent flow field. The transformation of the wake, from a well defined helicoidal vortical structure to a chaotic state, happens by the creation of secondary structures (see Fig. 1).

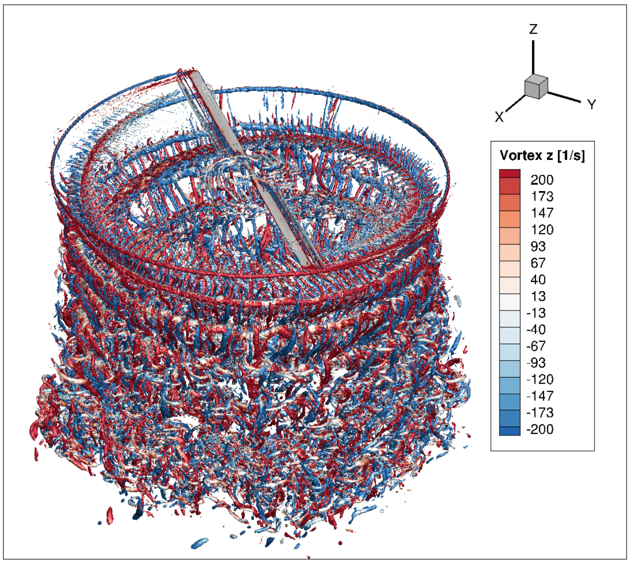

Figure 1: $\lambda_2 = -0.3$ iso-surface of the 2 blade rotor wake colored through the vertical vorticity magnitude.

These vortices feature a vertical axis, a lower circulation with respect to the MTV, and they are created from the entrenchment of the shear layer. The main feature of these vortices is the s-shape structure and they typically appear as couples of counter-rotating vortices. These secondary structures, firstly observed in high fidelity numerical simulations (Hariharan et al. [2], Abras et al. [3]), were later found experimentally by Wolf et al. [4] with PIV measurements. (??)

The MTV, on the other hand, has been analysed in detail through a number of studies such as Kindler et al. [5], Mula et al. [6], Martin and Leishman [7], Leishman [8]. It evolves from the blade tip and, due to the interactions with the blade shear layers, eventually decays in the chaotic pattern exposed before. The transformation of the wake, from a well defined helicoidal vortical structure to the turbulent state is still not fully understood. In fact, the mechanism of decay is a particularly complex topic because it involves not only possible macroscopic instabilities of the MTV helix (see Okulov and Sorensen [9] and Jain and Conlisk [10]), but also viscous mutual effects due to vortex interactions.

Moreover, difficulties in detecting the wake system of a rotor is a well known problem also for early wake ages, especially in experimental campaigns (Leishman et al. [11]). Effort to understand the wander of the MTV, so the spatial movements of the helix filament, is an outstanding practical question of great scientific interest. Correction techniques for experimental purposes have been proposed, see McAlister et al. [12] or Ramasamy et al. [13]. These spatial movements are strongly related to external factors, such as background turbulence (cfr. Kinder et al. [5]), so at late wake ages they become stronger and possibly fundamental for the rotor wake decay and for the creation of the secondary structures.

Therefore, providing an accurate method that allows to study the MTV at very late wake ages in high fidelity numerical simulations is of great scientific value. Though similar attempts have been done, with particular focus on the vortex core growth (see Kao et al. [14] or Kao et al. [15]), finding a method to correctly and automatically detect the vortex in difficult conditions very far form the rotor plane is still a great challenge. This work is devoted to illustrate a possible way to automatically detect the MTV of a rotor in hover through a clear and easily applicable procedure.

3. GEOMETRICAL AND NUMERICAL SETUP

The geometry considered is the same as the one presented by Heintz et al. [16]. The rotor is in hover and it is hold on a solid support, as shown in Fig 2. Different number of blades are considered, namely 1, 2 and 4.

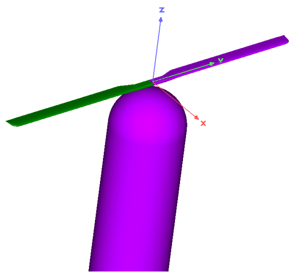

Figure 2: Geometry of the 2 blade rotor.

For the one blade case, an approximately 12 cm long cylindrical counterweight is mounted on the opposite side of the blade to compensate for the imbalance of the loadings. The blades are the commercial BlackBelt 685, which were already used in the experimental and numerical studies of Wolf et al. [4], Bodling et al. [17] and Schwarz et al. [18]. The SpinBlades are commercially available and they present a symmetrical airfoil and a parabolic tip shape. The chord length is $C = 0.061\ m$, the span is $0.685\ m$ and no twist is applied. In total, considering also the rotor hub, the tip radius is at $R = 0.760\ m$. Therefore, the solidity σ of the rotors are 0.0128, 0.0255 and 0.0511 for the 1, 2 and 4 blade rotor respectively. The angular velocity of the main rotor is $\omega = 118.44\ rad/s$ yielding a blade tip Mach number of $Ma = 0.26$.

The blade pitch is adjusted to achieve a blade loading of $C_T/\sigma = 0.085$.

The numerical investigation is based on the block structured finite volume RANS CFD code, FLOWer, developed by the German Aerospace Center (DLR) and improved for rotorcraft simulations by the research group at the Institute of Aerodynamics and Gasdynamics (IAG) in the University of Stuttgart. The solver is a finite volume code based on a 6^{th} order spatial discretization WENO (Weighted Essentially Non-Oscillatory, see Liu et al. [19]) and 2^{nd} order temporal discretization. Simulations are computed with a DDES-SST($k-\omega$) scheme.

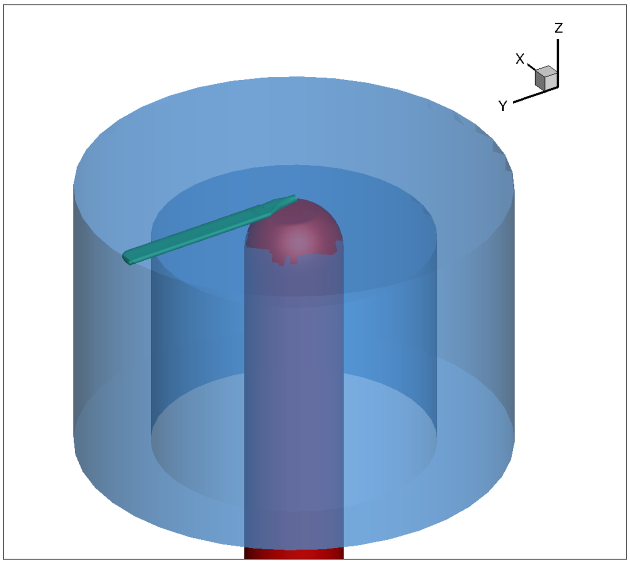

Figure 3: Different regions of the domain: green is the blade, red is the displacement body and light blue is the $2\%\ C$ refinement of the background mesh.

The structured mesh is used jointly with a Chimera technique. As illustrated in Fig. 3, the mesh is subdivided in regions. The first one is highlighted in green and it is close to the blade: it is devoted to the boundary layer computation. A similar one is created on the surface of the displacement body in the center, the red zone. The refinement of $2\%\ C$ on the background is highlighted in light blue. This region is composed of constant size cells.

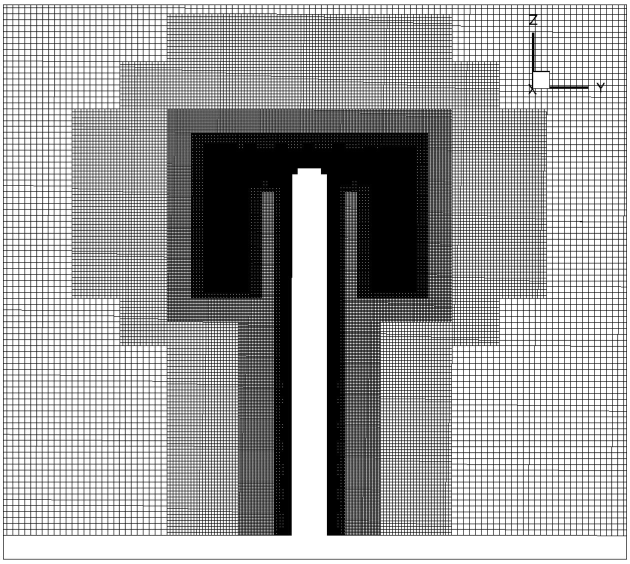

Figure 4: Mesh refinement.

All these regions are immersed in a background mesh which progressively increase the size of the elements towards the edged of the domain (which is located at $20 \cdot R$) in order to save computational power. The exchange of information among the regions described so far and between the refinement and the outer background are achieved through interpolations.

The regions close to the surfaces, the red and blue in Fig. 3, are created allowing a $y^+ = 1$ value at the wall. Regarding the light blue region of refinement, as reported in Fig. 4, a toroidal shape has been considered. The shape has been chosen to enclose the region where the wake decay is expected.

The sizes of the refinement region are $0.7 \cdot R$ in spanwise direction and $1.4 \cdot R$ below the rotor plane. The most of the cells are concentrated in this portion of space so the computational effort is only slightly affected by the different number of blades of the rotor. The main properties of the test-cases are reported in Table 1.

Test-case	**cells [10^6]**	**blocks**
1 blade	287.9	36532
2 blades	289.5	36666
4 blades	292.0	37052

Table 1: Test-cases meshes.

4. METHOD

The detection of the MTV is based on the study of the λ_2 criterion computed on the numerical solution. The workflow is presented below:

- Vortex detection criterion: λ_2 criterion
- $\overline{\lambda_2}$ threshold
- Choice of the initial point (r_0, z_0)
- Tracking method
- Stop criterion
- Vortex core shape

The procedure hereafter briefly presented is applied at different time instances during a complete revolution of the rotor.

4.1. Vortex detection criterion

The effort to track the vortex position is based on the determination of the proper criterion for the vortex identification. A number of studies have been proposed (Chakraborty et al. [20]). However, a unique and generally accepted definition of what is a vortex is an old problem not fully resolved still nowadays (cfr. Jeong and Hussain [21] or Hunt et al. [22]).

The intuitive ways to measure vortices, i.e. local pressure minimum, pathlines or streamlines and vorticity magnitude have been proved to be all not enough for a correct detection of vortical regions. Most common vortex identification method, such as λ_2 and Q criterion, are based on the gradient of the velocity instead.

In particular, the λ_2-criterion is based on the eigenvalues of the tensor $\mathbf{J} = \mathbf{S}^2 + \mathbf{\Omega}^2$ and considers the effects of both the rotation and the strain in the fluid. The tensors $\mathbf{S}$ and $\mathbf{\Omega}$ are the symmetric and anti-symmetric part of the tensor $\nabla \mathbf{u}$ respectively. It is worth recalling that the vortex core regions have a negative λ_2.

The absolute value of λ_2 is highly case dependent. To account of compressible effects, in this work the λ_2-criterion is computed starting from velocities expressed as Mach number ($M = u/a_{\text{inf}}$, $a_{\text{inf}} = \sqrt{\gamma R T_{\text{inf}}}$). Thus, all the considerations that will be presented below are based on λ_2 values having order of magnitude 10^{-1}.

4.2. Choice of $\overline{\lambda_2}$

In order to detect the vortices in the flow field, a threshold value $\overline{\lambda_2}$ must be defined. Due to the chaotic flow field, the right choice of the threshold becomes fundamental for the correct tracking of the MTV. The main problem related to an excessively low value of $\overline{\lambda_2}$ is usually the joining of different vortices into bigger nonphysical connected regions of no practical value. The risk is strongly increasing at late wake ages where the rotor wake has the aforementioned vortical complexity.

In order to select the most appropriate value of the threshold $\overline{\lambda_2}$, the suggestion is to use the smallest absolute value for $\overline{\lambda_2}$ in cleaner setups, such as the 1 blade case. On the other hand, rotors with a more complex flow field should to be associated with higher absolute values of $\overline{\lambda_2}$.

We propose to use the following empirical formula to estimate $\overline{\lambda_2}$:

$$\overline{\lambda_2} = -\frac{1}{7} \cdot \Gamma_{max} \cdot N_b. \tag{1}$$

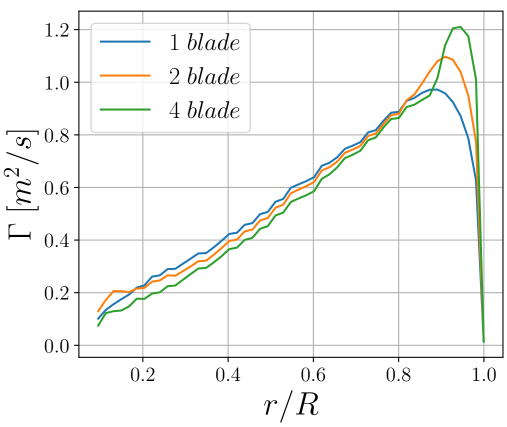

Figure 5: Span-wise blade circulation.

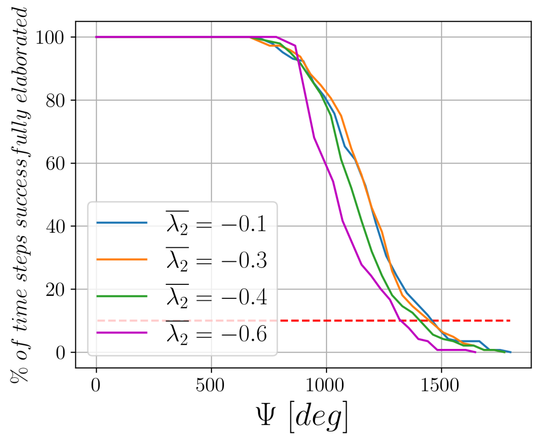

Figure 6: Number of instances of time with valuable results w.r.o. the wake age for different $\overline{\lambda_2}$.

where Γ_{max} is the maximum circulation on the blade in the span-wise direction, as shown in Fig. 5, while N_b is the number of blades. The circulation is computed with the Kutta-Joukowski theorem as $\Gamma(r/R) = L(r/R)/(\rho \cdot U(r/R))$ and it is an estimate of the MTV strength. In addition, in order to consider also the vertical distance between MTV coming from different blades, the number of blades N_b is taken into account in Eqn. 1.

Due to the fact that the procedure is computed independently at different time instances and the results are averaged along a whole revolution, the influence of the threshold is considered for each of these instances. Figure 6 shows, for each wake age Ψ and for the 2 blade rotor, the percentage of time instances where the MTV tracking is fully elaborated. The influence of $\overline{\lambda_2}$ in this detection is to slightly decrease the Ψ_{decay}, namely the maximum wake age at which it is possible to identify the MTV, for all time instances (violet line w.r.o. the orange line in Fig. 6). This it due to the fact that an excessively low value of $\overline{\lambda_2}$ increases the possibility of joining two close regions, thus stopping the detection method too early. On the other hand, increasing the value of $\overline{\lambda_2}$ reduces the complexity of the wake, thus the possibility of detecting very weak vortical structures such as the MTV at late wake ages. Thus, an optimum has to be found, in this case of the 2 blade rotor it is $\overline{\lambda_2} = -0.3$.

To conclude, the dotted line at 10% in Fig. 6 is representing the minimum number of time instances that has to be resolved under which the results are not considered meaningful anymore.

4.3. Choice of $(\mathbf{r_0}, \mathbf{z_0})$

The choice of the initial vortex position is very important in order to correctly follow the MTV. To have a more robust method, the first radial slice considered is at $\Delta\Psi = 5°$ downstream of the blade position. This allows to have an already well defined MTV, as illustrated in the radial section of the 1 blade rotor case in Fig. 7. Here, the initial position of the MTV is the higher blue region of negative λ_2 while the other branches of the MTV helix are visible below. The vortex decay is acting both as an increase of the vortex core dimensions and a decrease of the strength of it (i.e. the circulation of the vortex $\Gamma(\Psi)$).

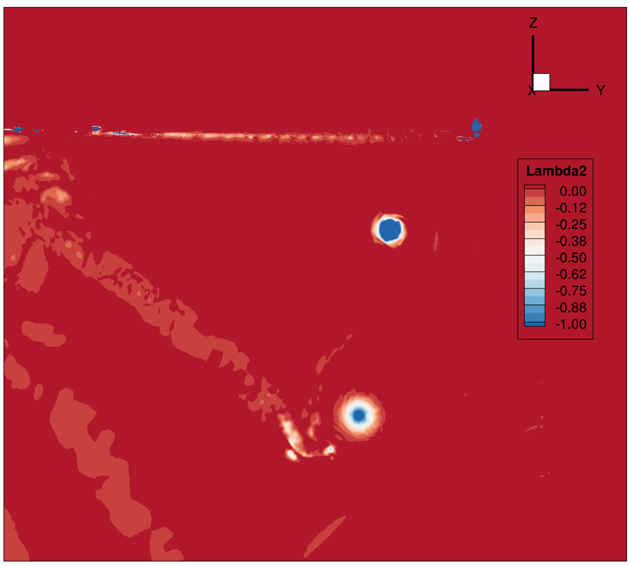

Figure 7: Radial section with λ_2 contour plot of the 1 blade rotor case.

4.4. Tracking method

The tracking of the MTV in the domain is based on the sampling of the computational domain in different radial sections, as reported in Fig. 8. The azimuth distance between sections has been taken as $\Delta\Psi = 1°$.

The tracking method is based on the detection of all the connected region in each section with $\lambda_2 \leq \overline{\lambda_2}$. For each of these connected regions, the center of gravity (CoG) of the λ_2-criterion is computed as:

(2) $$r_{CoG} = \sum_{i=1}^{N} (r_i - r_c) \cdot \lambda_2(r_i)$$

(3) $$z_{CoG} = \sum_{i=1}^{N} (z_i - z_c) \cdot \lambda_2(z_i)$$

where N is the total number of point of each connected region and (r_c, z_c) is the point where λ_2 is maximum. The distance between the center point computed through the maximum of λ_2 and the CoG is never more that $0.5\%\ R$.

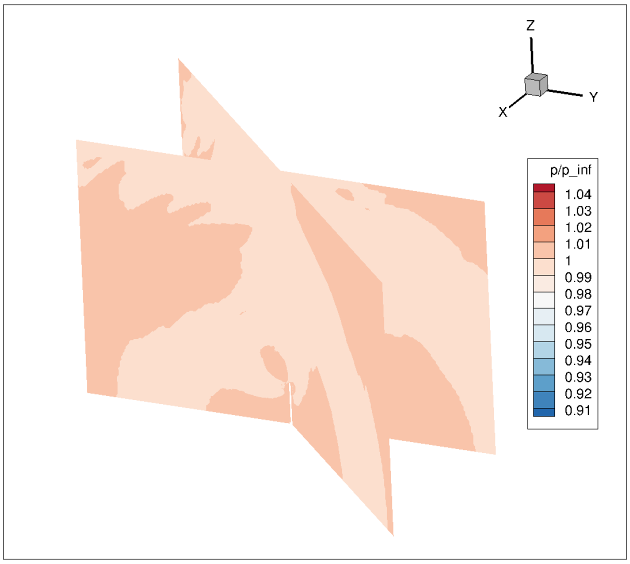

Figure 8: Radial sections example in the domain.

Once defined the CoGs of all the vortices and the initial point (r_0, z_0), it is possible to follow through the domain the position of the MTV considering sequentially the different radial sections. For each point, the closest among all the CoGs in the subsequent radial section is chosen by means of the smallest euclidean distance. Other possible more sophisticated criterion, such as λ_2 continuity or vorticity direction continuity between following CoGs are giving the same results but with increasing computational cost and complexity of the post-processing workflow.

4.5. Stop criterion

Following the MTV with the tracking method exposed so far is not enough to allow the right detection of the MTV. Unfortunately, no robust criterion has been proposed so far *a priori* to understand whether the procedure is following the right vortex or secondary structures. In Fig. 9 an example of the problem is shown: the detection of the MTV in the 2 blade rotor case is correctly performed up to a point where a wrong helix branch is followed.

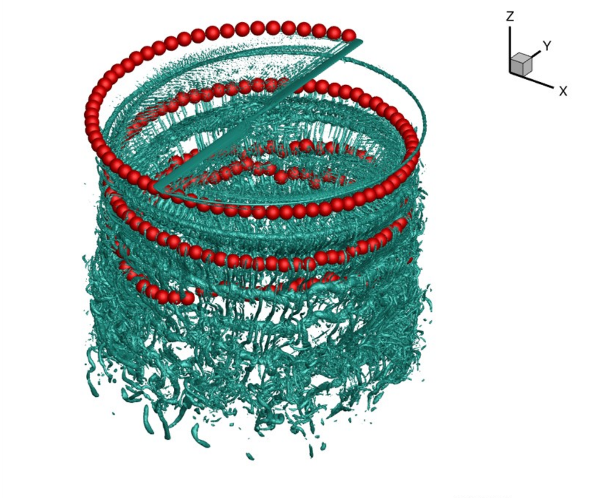

Figure 9: 2 blade rotor wake and detected MTV (red dots).

The solution to the problem is to consider the standard deviation Σ on the radial and axial positions of the MTV, as reported in Fig. 10. Here, the standard deviations are illustrated for the 3 different test-cases while changing the wake age. They present a monotone increase followed by a sudden jump after a certain wake age.

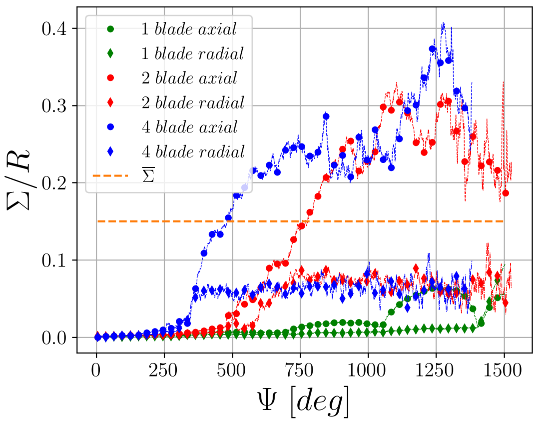

Figure 10: Standard deviation of the MTV positions.

This sudden increase of standard deviation, which is visible for the 2 blade and the 4 blade rotors (blue and red lines in Fig. 10), is located at $\Psi \approx 730°$ and $\Psi \approx 380°$ respectively. The meaning of this step increase is related to the impossibility, for the detection method, to detect the correct MTV instead of secondary vortical structures that increasingly degrade the vortex itself.

Thus, to avoid nonphysical values, a threshold $\overline{\Sigma}$ on the standard deviation Σ has been fixed: we propose here to choose as a threshold $\overline{\Sigma} = 0.15 \cdot R$. Values of Σ above this threshold are discarded. Therefore, the 2 blade rotor detection method is stopped at $\Psi = 758°$ while the 4 blade rotor at $\Psi = 482°$, which are in line with the experimental results of A. Heintz [personal communication]. The 1 blade rotor, instead, is never presenting $\Sigma \geq \overline{\Sigma}$ and, thus, no stop criterion is applied.

4.6. Shape of the MTV

An estimate of the cross-section shape of the MTV can be computed through an eigenvalue analysis of the covariance matrix associated to the the connected region of the vortex. In particular, the covariance matrix Ξ is computed as:

$$\Xi = \frac{1}{N-1}\sum_{i=1}^{N} \mathbf{C}_i \mathbf{C}_i^T \tag{4}$$

with $\mathbf{C_i}$ defined as

$$\mathbf{C}_i = \begin{bmatrix} r_i - \overline{r} \\ z_i - \overline{z} \end{bmatrix} \tag{5}$$

where $\overline{r}$ and $\overline{z}$ are the mean values on the connected region. The procedure allows to define an ellipse representing the approximated shape (95% confidence) of the connected region such that the square root of the eigenvalues of Ξ, namely Λ, are the semi-major axes while the eigenvectors represent the orientation of the ellipse.

5. RESULTS

The 3 different test-case analysed are reported in Table 2: while the blade loading C_T/σ is kept constant in order to have comparable wake decay processes, $\overline{\lambda_2}$, as defined in Section 4, is changing.

	α [deg]	T [N]	$\mathbf{C_T/\sigma}$	$\overline{\boldsymbol{\lambda_2}}$
1 blade	9.3	35.97	0.08	-0.1
2 blades	10.3	74.60	0.08	-0.3
4 blades	12.3	153.75	0.08	-0.7

Table 2: Test-cases results.

All the results presented below are averages of solutions computed at different time instances.

5.1. MTV positions

The position of the main tip vortex, in terms of axial and radial position, at different wake ages from the blade passage, are computed. The results are compared with the approximated solution proposed by Landgrebe [23]. In particular, the following relations are used:

$$\frac{y}{R} = \begin{cases} k_1\Psi & \text{if } 0 \leq \Psi \leq \frac{2\pi}{N_b} \\ \left(\frac{y}{R}\right)_{\Psi=2\pi/N_b} + k_2\left(\Psi - \frac{2\pi}{N_b}\right) & \text{if } \Psi > \frac{2\pi}{N_b} \end{cases} \tag{6}$$

$$\frac{r}{R} = A + (1-A)e^{-\eta\Psi} \tag{7}$$

where k_1 and k_2 are related to C_T/σ and C_T as:

(8) $$k_1 = -0.25(C_T/\sigma + 0.001\theta_t)$$

(9) $$k_2 = -(1.41 + 0.0141\theta_t)\sqrt{(C_T/2}$$

while A = 0.78 and η = $0.145 + 27C_T$. θ_t is the twist angle: in our case $\theta_t = 0$

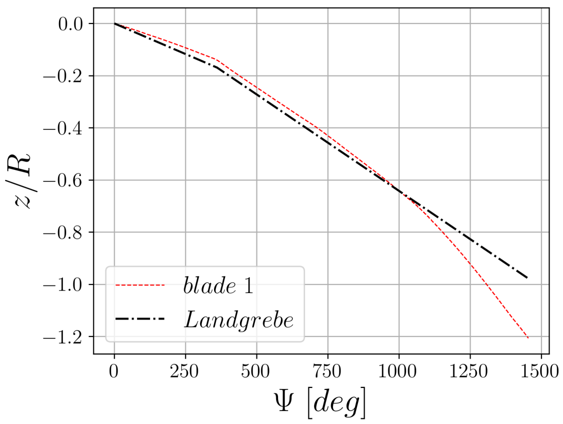

Figure 11: Axial position of the MTV for the 1 blade rotor.

In Fig. 11 and Fig. 12 the comparison between computed and approximated positions for the 1 blade rotor is shown. For the axial position, a good agreement between methods is retrieved up to $\Psi = 1000°$. The first blade passage, in this case at $\Psi = 360°$, is increasing the pitch of the helix as expected (higher slope of the curve). The approximated solution of Landgrebe, which forecasts a constant pitch of the helix even far from the blade, is above the computed values from $\Psi = 1000°$. Regarding the radial position, the approximated solution is accurate also at very high wake ages Ψ.

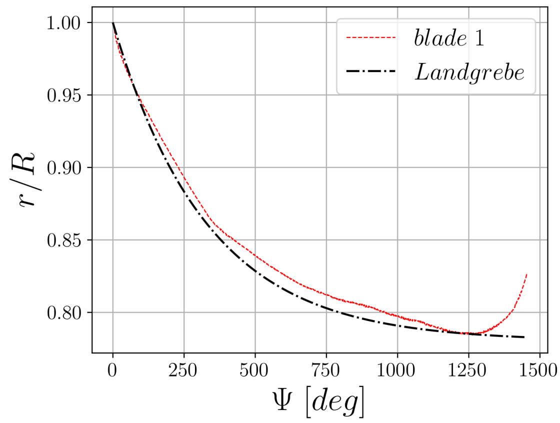

Figure 12: Radial position of the MTV for the 1 blade rotor.

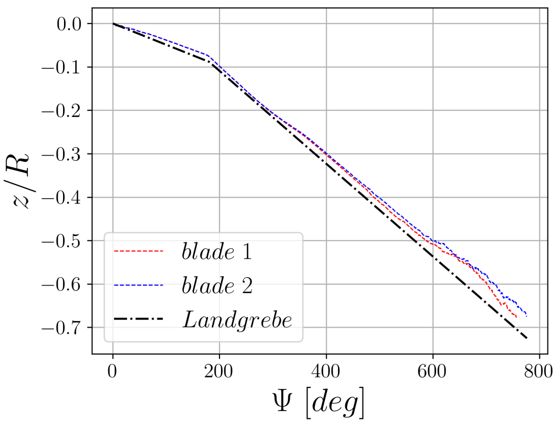

Figure 13: Axial position of the MTV for the 2 blade rotor.

The 2 blade rotor test-case (see Fig. 13 and Fig. 14) is presenting a similar behaviour. The 2 blades MTV are studied separately. Now, the first blade passage is at $\Psi = 180°$, as highlighted by the change of slope of the axial position. The solution of Landgrebe is slightly lower than the numerical one. The presence of the 2 different MTV allows to find vortex pairing, namely the asymmetric shape of the wake due to the mutual inductance of the vortices. This result was unexpected and was only due to vortex dynamics; the setup, in fact, is perfectly symmetric. The pairing of the vortices is stronger in the radial direction and between $\Psi = 300°$ and $\Psi = 750°$.

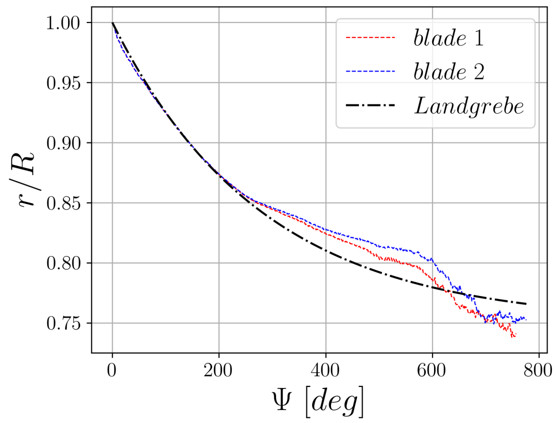

Figure 14: Radial position of the MTV for the 2 blade rotor, the vortex pairing is visible for $\Psi \geq 400°$.

To conclude, Fig. 15 and Fig. 16 present the results for the 4 blade case. Here, no clear pairing is visible but at very late wake ages, where the radial positions start to become very unstable.

Due to the fact that all these results are averages on a whole rotor revolution, a standard deviation Σ on the position can be computed. The wandering of the MTV, namely the spatial fluctuations of the MTV, can be analysed with this standard deviation, following the approach of Kindler et al. [5]. The wandering, which is caused by external perturbations such as background turbulence (see Heyes et al. [24]), is, in general, increasing continuously (see Fig. 17).

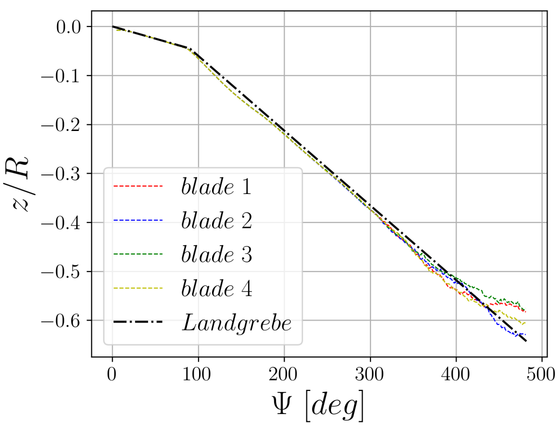

Figure 15: Axial position of the MTV for the 4 blade rotor.

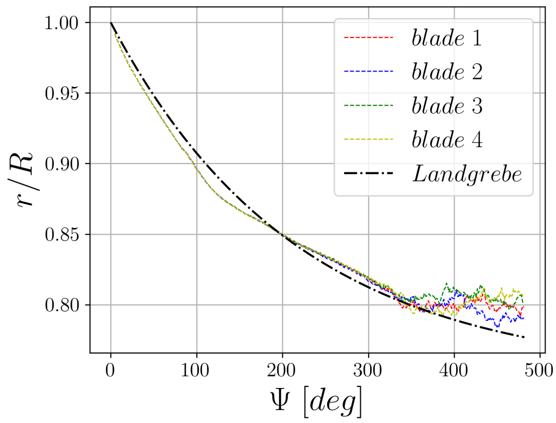

Figure 16: Radial position of the MTV for the 4 blade rotor.

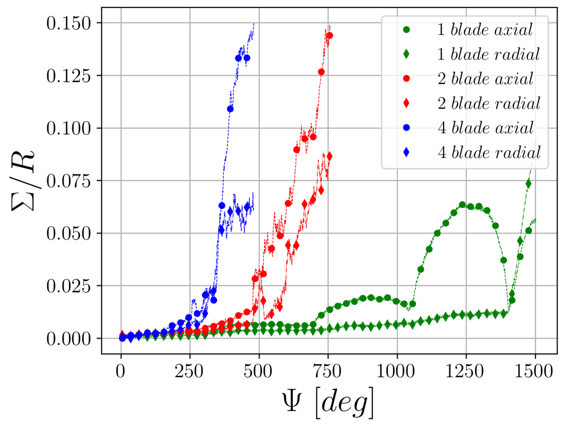

Figure 17: Wandering of the MTV, expressed as the standard deviation Σ of the position.

In Fig. 17 it is presented the comparison between the 3 different test-cases. As reported also in Kindler et al. [5] for the near field ($\Psi \leq 30°$) MTV development, the wandering is stronger in the axial direction than in the radial one. This is valid for all the cases (dot w.r.o. diamond marks) but becomes strongly visible at later wake ages Ψ. The 1 blade rotor (green lines) is presenting a Σ value that is strongly affected by the Blade Passage Frequency BPF (in this case $\Psi = 360°$, $\Psi = 720°$ and so on). In particular, each time these wake ages are reached, Σ of the axial position increases and then decreases again, giving a "wave" trend to the curve. The mechanism is enhanced from the second blade passage on. The radial value of Σ is less affected by the BPF, which is reasonable because the effect is related to a downwards movement of the MTV. The increase of the axial wandering is present also for rotors with more blades. Again, the increase is stronger after the second blade passage and it eventually leads to the step on the standard deviation σ, so the decay of the MTV. The mechanism is reasonable and is related to the lower distance between the MTV filaments (more blades): an axial movement of the vortex leads to a merging and a fading of the vortex itself.

In the near wake solutions ($\Psi \leq 250°$), the standard deviation is shown in Fig. 18. The 1 blade rotor is presenting lower values of Σ (green dots) than the other rotors. Moreover, it presents a clear smaller wandering in the radial direction than in the axial one. This is less evident at these ealry wake ages for the 2 and the 4 blade rotors. The increasing of the axial wandering after the second blade passage is evident for the 4 blade rotor for $\Psi \approx 180°$ (blue dots).

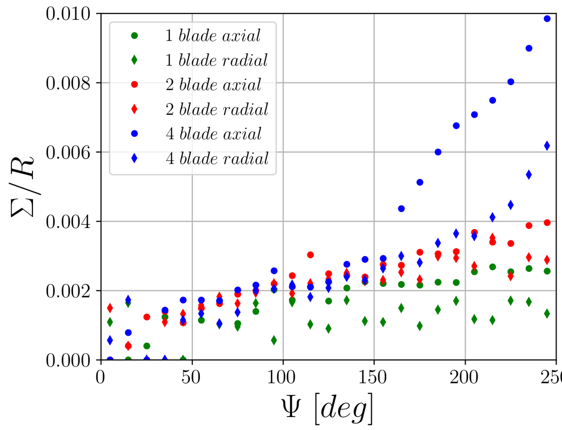

Figure 18: Wandering of the MTV, expressed as the standard deviation Σ of the position: detail for $\Psi \leq 250°$.

5.2. Circulation

The circulation Γ of the MTV is computed, for each wake age Ψ, as:

$$\Gamma(\Psi) = \oint_{\xi} \mathbf{U} \cdot d\mathbf{l} \tag{10}$$

where ξ is a closed circular path, $\mathbf{U}$ is the velocity and $d\mathbf{l}$ is the infinitesimal tangential versor of the path ξ.

Fig. 19 shows the circulation on the 1 blade rotor test-case as computed with different radius R_ξ of the integration path ξ. Increasing the radius, the circulation converges to a more constant trend while changing the wake age Ψ (red symbols as compare to blue ones).

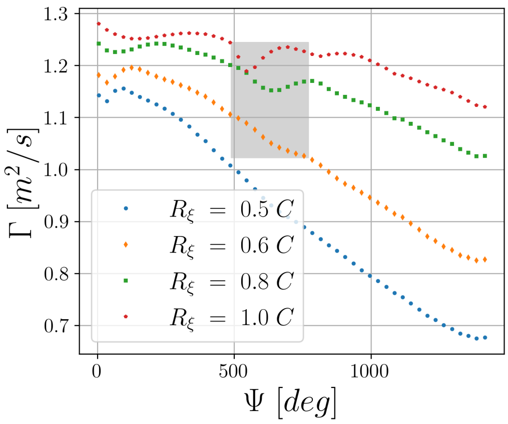

Figure 19: Circulation of the MTV for the 1 blade rotor.

This is due to the fact that the MTV dimensions increase during the decay so keeping constant R_ξ does not allow to consider all the circulation of the vortex. On the other hand, increasing R_ξ for all wake ages introduces a drop on the computed circulation (grey zone in Fig. 19). This drop is related to the shear layer vorticity, which enters inside the integration path as shown in Fig. 20. In particular, the circle of integration of $R_\xi = 1.0 \cdot C$ (red line) is clearly considering also the effects of the shear layer. Therefore, the results in the grey zone of Fig. 19 mujst be treated carefully.

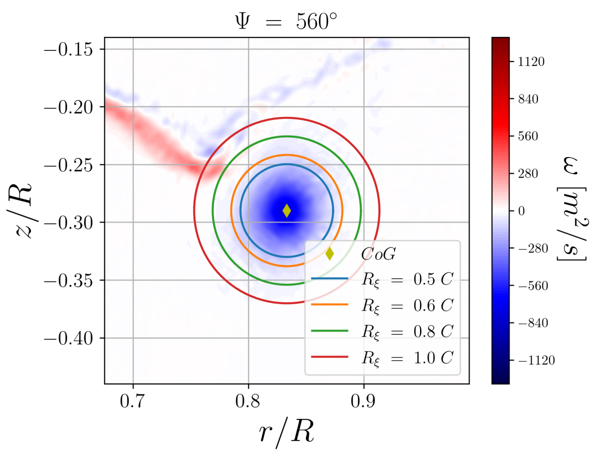

Figure 20: Out of plane vorticity at $\Psi = 560°$ for the 1 blade rotor and corresponding R_ξ.

Similar considerations can be done on the circulation of the 2 blade rotor (see Fig. 21). Here the circulation is less affected by R_ξ while the drop is more heavily affected by the shear layer (grey zone). Moreover, the circulation is strongly decaying for $\Psi \geq 600°$ proving that the stop criterion presented in Section 4 correctly avoids nonphysical results.

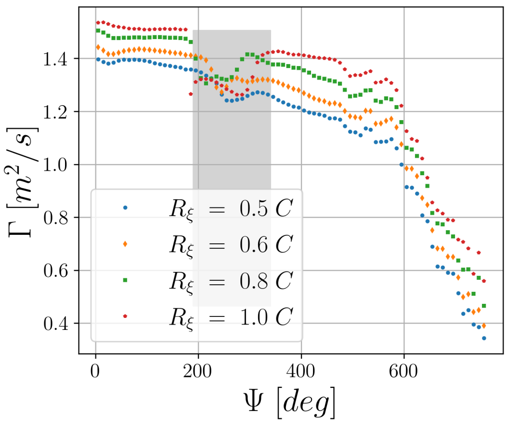

Figure 21: Circulation of the MTV for the 2 blade rotor.

The drop in circulation for the 2 blade rotor (grey zone) is more evident than with the 1 blade rotor. This is due to the fact that the shear layer effect on the MTV circulation computation occurs at a lower wake age than the case of the 1 blade rotor ($\Psi \approx 190°$ instead of $\Psi \approx 490°$). Therefore, the shear layer is less dissipated in the 2 blade rotor, as shown in Fig. 22.

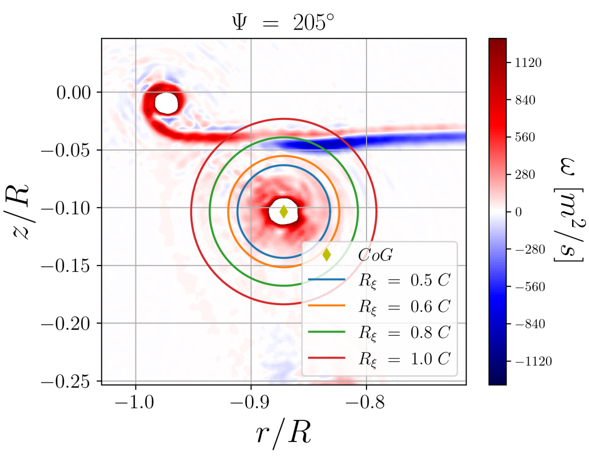

Figure 22: Out of plane vorticity at $\Psi = 205°$ for the 2 blade rotor and corresponding R_ξ.

To conclude, Fig. 23 is presenting the circulation for the 4 blade rotor.

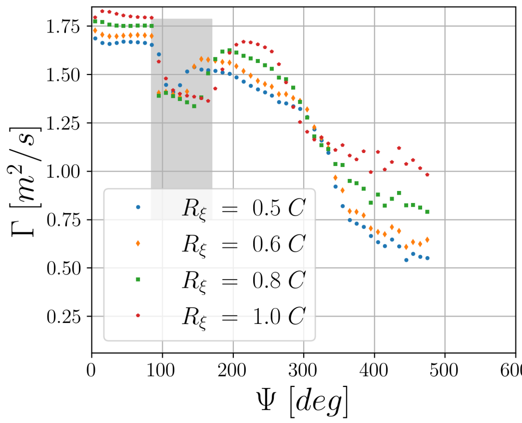

Figure 23: Circulation of the MTV for the 4 blade rotor.

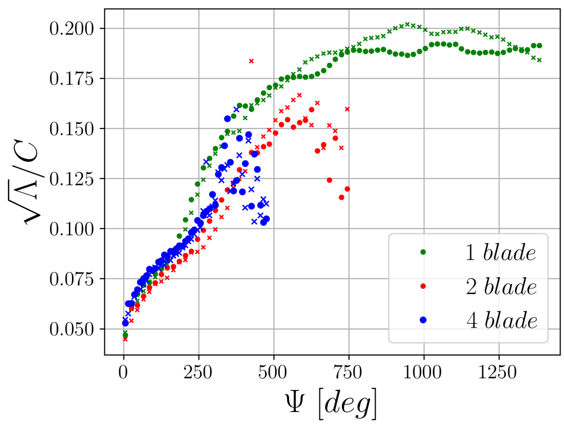

Figure 24: Eigenvalues Λ computed for the different test-cases.

5.3. Vortex shapes

To study the shape of the MTV while changing wake age Ψ, the eigenvalue analysis of the covariance matrix of the corresponding connected region has been computed, as reported in Section 4. In particular, the square root of the eigenvalues, Λ_1 and Λ_2, are representative of the semi-major axis of an ellipse approximating with 95% confidence the connected region of interest. In Fig. 24 the comparison between the 3 different test-cases has been reported. The 1 blade rotor (green symbols) is presenting 2 eigenvalues (cruxes and dots) of different amplitude at late wake ages, so $\Psi \geq 600°$. Thus, the MTV vortex is stretched after an initial development where it is more circular. Increasing the number of blade, the MTV has eigenvalues Λ of comparable size. Therefore, the vortices are presenting a more circular cross section (smaller eccentricity).

A typical approach for analysing the vortex growth is the Normalized Vortex Core Diameter (NVCD), defined as the ratio of the core diameter and the rotor blade tip-chord (see Kao et al. [15]). However, due to the deformed shape of the vortex core, the definition of a core diameter is difficult to give.

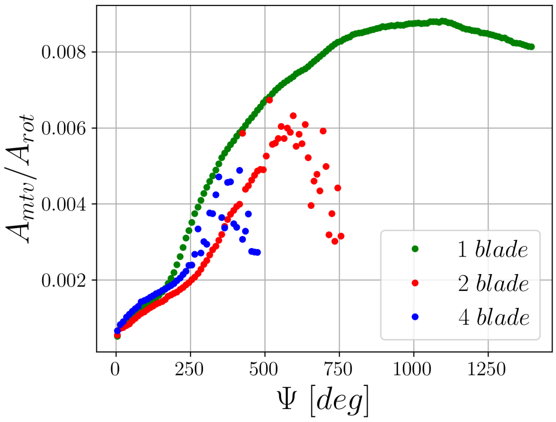

Figure 25: Area of the MTV for the different test-cases.

Thus, an alternative estimation for the MTV area can be computed from the area of the approximated ellipse as $A_{MTV} = \pi \cdot \sqrt{\Lambda_1} \cdot \sqrt{\Lambda_2} \cdot 5.991^2$; 5.991^2 is the Chi-squared valued to achieve 95% confidence with 2 variables. In Fig. 25 it is illustrated how the area of the MTV increases up to a certain point where the vortex decays. The maximum of area is dependent of the test-case. It is remarkable that the 2 blade rotor (red symbols) presents the less spread MTV.

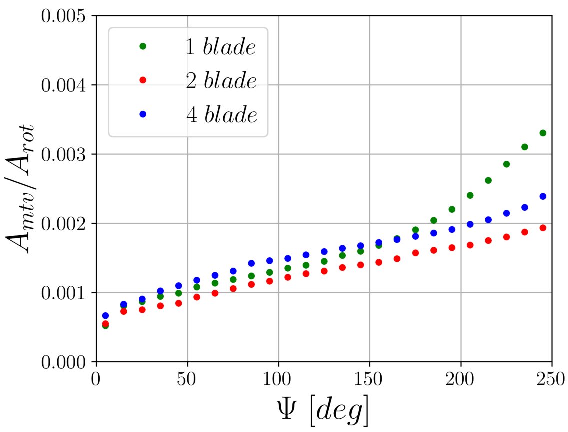

Figure 26: Detail of the area of the MTV for the different test-cases.

It is also interesting to analyse the trend of the vortex area for $\Psi \leq 250°$ (see Fig. 26). The monotonic increase in this near wake region is presenting higher values of area for the 4 blade rotor (blue symbols) than the other test-cases. However, the 1 blade rotor (green symbols) is overcoming the other 2 rotors from $\Psi \approx 180°$, from which it has the most spread MTV by far (almost 3 times more than the 2 blade rotor). This explains why changing the integration radius R_ξ for computing the circulation affects more the 1 blade rotor with respect to the other ones.

6. CONCLUSIONS

A detection method to automatically track the main tip vortex (MTV) in a rotor in hover has been presented. Difficulties arise due to the chaotic, turbulent and unsteady flow field characteristic of decaying rotor wakes.

Thus, to allow the correct detection of the MTV, a number of precautions has been developed in order to achieve the most reliable results even at very late wake ages. In particular, the choice of the threshold $\overline{\lambda_2}$ is important for a correct detection of the vortex regions in the flow field. Moreover, the euclidean distance has proved to be the easiest and most reliable way to follow the MTV on the domain. However, the procedure is not enough to achieve valuable results due to the possibility of introducing errors in the tracking. To avoid it, a stop criterion has been introduced. It is based on the computation of the standard deviation Σ of the MTV position through the definition of a threshold $\overline{\sigma}$: all the results lying above the threshold are discarded as physically meaningless.

The results computed for the test-cases, namely a rotor in hover with different number of blades, has highlighted a good agreement with prediction found in literature. Remarkably, there is a connection between wandering, namely spatial fluctuation, of the MTV and the Blade Passage Frequency (BPF). In particular, the connection between the increase of the standard deviation Σ in axial direction and the decay of the MTV itself in rotor with more than 1 blade is enhanced after the second blade passage.

Regarding the circulation computation, a strong dependency on the radius of integration R_ξ has been found. Moreover, even though an increase in the integration radius is beneficial to capture all the vorticity related to the MTV, a problem can arise due to the presence of the shear layer. This is particularly relevant increasing the number of blade of the rotor and it leads to a nonphysical drop on the circulation close to the first BPF.

The different influence of the integration radius R_ξ on the circulation is related to the shape and size of the MTV. Thus, the eigenvalue analysis of the covariance matrix of the connected region of the vortex can be performed. From this analysis, an approximated ellipse of 95% confidence is computed. This allows to estimate the distortion of the vortex, which is lower for rotors with more blades. In conclusion, this analysis allows to find that the MTV of the 1 blade rotor is more spread with respect of the other 2 test-cases.

Author contact:
Filippo Gajo, filippo.gajo@iag.uni-stuttgart.de

7. ACKNOWLEDGMENTS

The author gratefully acknowledge the support provided by the Institute of Aerodynamics and Gasdynamics (IAG) of the University of Stuttgart for their support as well as the the DLR of Göttingen group. In particular, I thank Alexander Heintz for all the valuable discussions.

8. References

1. N. Chaderjian and P. Buning, "High resolution navier-stokes simulation of rotor wakes.," *Annual Forum Proceedings - AHS International*, vol. 1, pp. 375–392, 01 2011.

2. N. Hariharan, T. Egolf, and L. Sankar, "Simulation of rotor in hover: Current state, challenges and standardized evaluation.," *American Institute of Aeronautics and Astronautics, National Harbor, MD*, 01 2014.

3. J. Abras, N. Hariharan, and R. Narducci, "Wake breakdown of high-fidelity simulations of a rotor in hover.," *American Institute of Aeronautics and Astronautics, San Diego, CA*, 01 2019.

4. C. Schwarz, A. Bodling, C. Wolf, D. Michaelis, K. Kaufmann, A. Gardner, and J. Bosbach, "Experimental study of secondary structures in a rotor wake," *45th Rotorcraft Forum*, 2019.

5. K. Kindler, K. Mulleners, H. Richard, B. Wall, and M. Raffel, "Aperiodicity in the near field of full-scale rotor blade tip vortices.," *Experiments in Fluids*, vol. Vol. 50, pp. 1601–1610, 06 2011.

6. S. Mula, J. Stephenson, C. Tinney, and J. Sirohi, "Dynamical characteristics of the tip vortex from a four-bladed rotor in hover.," *Experiments in Fluids*, vol. 54, 10 2013.

7. P. Martin and J. G. Leishman, "Trailing vortex measurements in the wake of a hovering rotor blade with various tip shapes.," 02 2003.

8. J. G. Leishman, "Measurements of the aperiodic wake of a hovering rotor.," *Experiments in Fluids*, vol. 25, pp. 352–361, 10 1998.

9. V. Okulov and J. Sørensen, "Instability of a vortex wake behind wind turbines," *Doklady Physics*, vol. 49, pp. 772–777, 12 2004.

10. R. Jain and A. Conlisk, "Interaction of tip-vortices in the wake of a two-bladed rotor in axial flight," *Journal of The American Helicopter Society - J AMER HELICOPTER SOC*, vol. 45, 07 2000.

11. J. G. Leishman and A. Bagai, "Challenges in understanding the vortex dynamics of helicopter rotor wakes," *AIAA Journal*, vol. 36, no. 7, pp. 1130–1140, 1998.

12. K. W. McAlister, "Rotor wake development during the first revolution.," *American helicopter society 59th annual forum, Phoenix, USA*, 05 2003.

13. M. Ramasamy, B. Johnson, T. Huismann, and J. Leishman, "Digital particle image velocimetry measurements of tip vortex characteristics using an improved aperiodicity correction," *Journal of the American Helicopter Society*, vol. 54, pp. 12004–1, 01 2009.

14. D. Kao, J. Ahmad, and T. Holst, "Visualization and quantification of rotor tip vortices in helicopter flows," *AIAA SciTech Forum*, 01 2015.

15. D. L. Kao, K. L. Smith, and Z. Liu, "Tracking blade tip vortices for numerical flow simulations of hovering rotorcraft," *AIAA Aerospace Sciences Meeting*, 2018.

16. A. Heintz, C. Schwarz, C. Wolf, and M. Raffel, "Influence of configurational parameters on the vortex system of a rotor in hover," *AIAA SciTech*

2024 Forum, American Institute of Aeronautics and Astronautics, Orlando, FL, 2024.

17. A. Bodling, C. Schwarz, C. C. Wolf, and A. D. Gardner, “Numerical and experimental assessment of parameters influencing the development of secondary vortex structures in rotor wakes,” *Proceedings of the Vertical Flight Society 79th Annual Forum, Vertical Flight Society, West Palm Beach, Florida USA*, 2023.

18. C. Schwarz, A. Bodling, C. C. Wolf, R. Brinkema, M. Potsdam, and A. D. Gardner, “Development of secondary vortex structures in rotor wakes,” *Experiments in Fluids, Vol. 63, No. 1*, 2022.

19. X.-D. Liu, S. Osher, and T. Chan, “Weighted essentially non-oscillatory schemes,” *Journal of Computational Physics*, vol. 115, no. 1, pp. 200–212, 1994.

20. P. Chakraborty, S. Balachandar, and R. Adrian, “On the relationships between local vortex identification schemes.,” *Journal of Fluid Mechanics*, vol. 535, pp. 189 – 214, 07 2005.

21. J. Jeong and F. Hussain, “On the identification of a vortex.,” *Journal of Fluid Mechanics*, vol. 285, p. 69–94, 1995.

22. J. Hunt, A. Wray, and P. Moin, “Eddies, streams, and convergence zones in turbulent flows.,” *Studying Turbulence Using Numerical Simulation Databases*, vol. -1, pp. 193–208, 11 1988.

23. J. A. Landgrebe, “The wake geometry of a hovering helicopter rotor and its influence on rotor performance.,” *Journal of the American Helicopter Society*, vol. 17, pp. 3–15(13), 10 1972.

24. A. Heyes, S. Hubbard, A. Marquis, and D. Smith, “On the roll-up of a trailing vortex sheet in the very near field,” *Proceedings of The Institution of Mechanical Engineers Part G-journal of Aerospace Engineering - PROC INST MECH ENG G-J A E*, vol. 217, pp. 262–268, 05 2003.